machines

MDPI

Article

Non-Magnetic Negative Coefficient of Thermal Expansion Support Structure between Payloads in the Taiji Space Gravitational Wave Detection Satellite

Yuqing Diao [1,2,3], Wei Tao [1,2,3], Xiaoqin Deng [1,2,3] and Wei Sha [1,2,3,*]

[1] State Key Laboratory of Applied Optics, Changchun Institute of Optics, Fine Mechanics and Physics (CIOMP), Chinese Academy of Sciences, Changchun 130033, China; diaoyuqing21@mails.ucas.ac.cn (Y.D.); taowei19@mails.ucas.edu.cn (W.T.); dengxiaoqin19@mails.ucas.edu.cn (X.D.)
[2] University of Chinese Academy of Sciences (UCAS), Beijing 100049, China
[3] Key Laboratory of Optical System Advanced Manufacturing Technology, Chinese Academy of Sciences, Changchun 130033, China
* Correspondence: shawei@ciomp.ac.cn; Tel.: +86-137-5688-3069

Abstract: The support structure between payloads is an important part of a space gravitational wave detection satellite, and its thermal stability will directly affect the interferometer's measurement accuracy. However, due to temperature changes, the connecting structure between the loads will generate deformation, and a support structure with the coefficient of thermal expansion (CTE) of -1×10^{-6}/K will thus need to be designed to counteract this thermal deformation. In order to solve this problem, this paper adopts the method of mutual offsetting of the thermal deformation of different materials to design a thermally stable support structure satisfying this negative CTE. The structure was optimized by the arithmetic of non-linear programming by the quadratic Lagrangian hybrid algorithm (NLPQL), and the structural parameter satisfying the CTE of -1.008×10^{-6}/K was obtained. Meanwhile, the effect of the change in the thermal expansion coefficient of each material on the overall structure under this parameter was sampled and calculated. Moreover, the experimental results show that the CTE of the support structure under the optimized parameters was -1.114×10^{-6}/K, which differs from the simulation results by 9.5%.

Keywords: athermalization; Taiji Program; space gravitational wave detection; support structures

Citation: Diao, Y.; Tao, W.; Deng, X.; Sha, W. Non-Magnetic Negative Coefficient of Thermal Expansion Support Structure between Payloads in the Taiji Space Gravitational Wave Detection Satellite. *Machines* **2023**, *11*, 948. https://doi.org/10.3390/machines11100948

Received: 11 September 2023
Revised: 7 October 2023
Accepted: 8 October 2023
Published: 11 October 2023

1. Introduction

Gravity waves are ripples in the spacetime structure predicted by Albert Einstein's theory of general relativity, constituting a form of a matter wave [1]. Gravitational wave detection is important for understanding the evolution of the universe and the formation of objects such as black holes and for verifying theories, such as general relativity [2,3]. In the field of gravitational wave detection, the ground-based gravitational wave observatory LIGO directly detected a gravitational wave event for the first time in 2016 [4]. However, due to the limitations of the low-frequency Earth vibration and the Earth's curvature, the detection frequency range can only cover 10 Hz~10^4 Hz [5,6]. The sources in this range primarily include black hole mergers with masses ranging from tens to hundreds of times that of our Sun and binary neutron star mergers, holding significant astrophysical and cosmological importance.

However, there are sources of gravitational waves with even deeper cosmic and astronomical significance, such as supermassive black holes with masses ranging from thousands to millions of times that of our Sun. These sources emit gravitational waves in the low- to mid-frequency range (0.1 mHz to 1 Hz) [1,2]. In order to obtain gravitational wave sources with higher red-shifts, larger scales at low and intermediate frequencies,

as well as gravitational wave measurement information of deeper cosmological and astronomical significance, space-based gravitational wave detection has become a more preferable option [7,8].

Against this background, the Chinese space-based gravitational wave detection project, the Taiji Program, was born. Its basic principle is to use a Michelson interferometer to measure the changes in the laser path caused by the stretching or compression of spacetime in the vicinity of the gravitational wave passages by means of heterodyne interferometry [9,10]. A Michelson interferometer is an optical device that splits and recombines light beams to measure small displacements and wavelengths through interference patterns. The basic in-satellite structure is shown in Figure 1, and it consists of a proof mass, an interferometer, a telescope, and its support structure [11]. The satellite's internal structures are used in pairs. The laser from the interferometer on the remote spacecraft passes through the telescope, and after 3 million kilometers, it will be accepted by the telescope on the other spacecraft to reach the local interferometer to interfere with the laser reflected back to the interferometer by the local proof mass [3,11]. However, temperature variations (about $\pm$0.1 K) in the space environment cause small deformations in the support structure, which in turn lead to small changes in the optical path. Because the gravitational wave signal is very weak, even very small variations in the optical path can overwhelm the measurement signal [12]. In order to achieve the goal of the Taiji Program, i.e., an interstellar ranging accuracy of 5–8 pm/Hz$^{1/2}$ [12,13], it is necessary that "the support system between the payloads has a thermal stability on the order of pm to ensure the stability of the measured optical path".

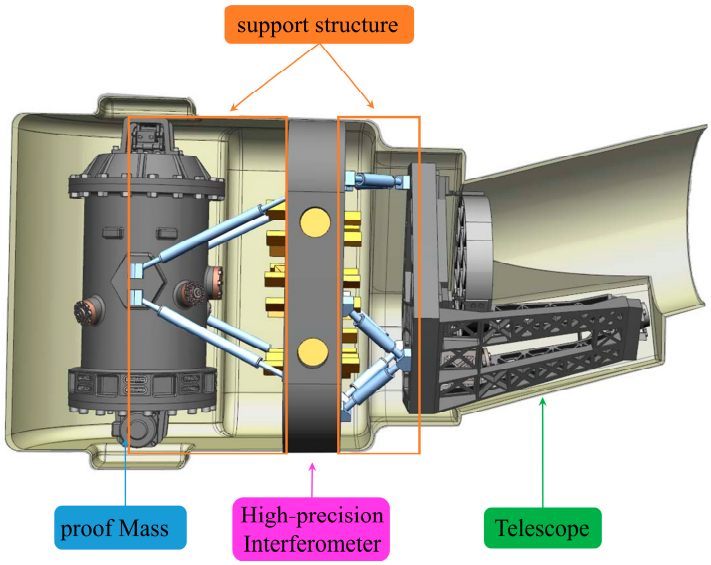

Figure 1. Basic structure inside the space gravitational wave detection satellite of the "Taiji Program".

However, the internal support structure of the Taiji Program is different from the traditional optical support structure. Firstly, it demands higher thermal stability (pm level), making traditional support materials like aluminum alloys and titanium alloys with relatively large coefficients of thermal expansion (CTEs) unable to meet the thermal stability requirements of the Taiji Program. For instance, the CTE of titanium alloy is approximately (8.6~10.03) $\times$ 10^{-6}/K, while aluminum alloy has a CTE in the range of (18~24) $\times$ 10^{-6}/K. Secondly, because the detection of gravitational waves in space is based on the detection between satellites, it requires the satellite platform to have as little as possible or even no magnetic moment to minimize the impact on the satellite attitude control [14,15]. Therefore, some materials with large magnetic moments, such as invar, cannot be applied to the support structure either. In addition, although carbon fiber-reinforced plastic (CFRP) can be used to obtain an ideal CTE for the support rod by adjusting the layup of the carbon fiber

material [16], due to the outgassing phenomenon of carbon fiber fabric (which is the release of gases absorbed or trapped, such as water vapor, during the CFRP production process), it can potentially have a significant impact on the dimensional stability of the structure [17]. Finally, the support structure is not used for the connection between components but for the connection between payloads. Therefore, it is necessary to consider not only the effect of reducing the thermal deformation generated by the support structure itself but also the thermal deformation that may be generated by the connection structure between each payload. Certainly, an actively adjustable support structure is also a good choice. However, its adjustment precision is relatively low (μm level) [18], and the vibrations that motors may generate could potentially introduce noise for space-based gravitational wave detection. Therefore, it cannot be directly used in the Taiji support structure.

Although excellent results have been achieved in temperature control, the temperature change rate of the core load in Taiji-1 has realized (T ± 0.1) K/1000 s, i.e., the temperature change during the working process of 1000 s is controlled within 0.1 K, and this slow temperature change ensures the temperature in the structure can be fully conducted. At the same time, the high-precision and high-stability temperature controller inside the satellite has been able to realize the temperature control accuracy index of (T ± 0.005) K (T is the calibration temperature), i.e., the fluctuation of the temperature uniformity inside the experimental box does not exceed ±0.005 K [19]. Therefore, it can be basically considered that a uniformly varying temperature field has been realized inside the satellite. Thus, the design of the support structure can be carried out in accordance with the uniformly varying temperature field.

Based on the above content, in this paper, we mainly carried out three aspects of work: (1) the support structure was designed with the combination of titanium alloy and aluminum alloy, the CTE difference in each material was used to improve the overall thermal stability of the support rod, and the initial parameters of the structure were obtained; (2) the whole structure of the rod was optimized by non-linear programming by the quadratic Lagrangian hybrid algorithm (NLPQL) [20], the CTE of the structural parameters that meet the requirements of the structural parameters was obtained, and the error caused by the change in the CTE of each material was calculated; and (3) in the ground temperature-controlled experimental box, the fiber-based interferometer and the temperature-controlled box were used to determine the thermal expansion coefficient of the support structure, and the actual overall thermal expansion coefficient of the structure was obtained. Through the above work, we hope to contribute to the successful implementation of the Taiji Program and the further development of the field of space gravitational wave detection. In the next phase, we will continue to explore the stress and strain mechanisms arising from the different CTEs of each material, aiming to further enhance the thermal stability of the support structure. Ultimately, our goal is to achieve the pm level of dimensional stability required for the Taiji Program.

2. The Design Process of the Taiji Support Structure

2.1. Specific Design Process

Although it is difficult for many single materials to meet the needs of the Taiji Program in a uniform temperature field, it is possible to use the different thermal expansion characteristics of the materials to produce a certain difference in the thermal expansion process. Meanwhile, by adjusting the length of the rod of different materials to obtain the specific difference in thermal expansion, this changes the CTE of the entire rod. At the same time, the slow temperature change allows the metal to conduct heat sufficiently so that the different materials reach the same temperature. According to Equation (1) for thermal expansion,

$$\Delta l = l \cdot \Delta T \cdot \alpha \quad (1)$$

Δl is the displacement change, l is the material length, ΔT is the temperature change, and α is the CTE of the material.

We designed the thermal expansion support rod as shown in Figure 2. One end of the rod is the reference end, and another rod of a different material, from the other end of the previous rod, is expanded in the opposite direction to counteract the thermal deformation of the previous rod. According to the difference in the thermal deformation of the different rods, the displacement of the whole rod relative to the moving end and the reference end can be controlled. Therefore, it is possible to realize an arbitrary CTE between the reference end and the relative moving end of the whole rod within a certain interval, and the CTE of the whole rod can be adjusted by adjusting the length of the sub-rod (i.e., the distance between the adjustment surfaces) within a certain range of the amount of adjustment.

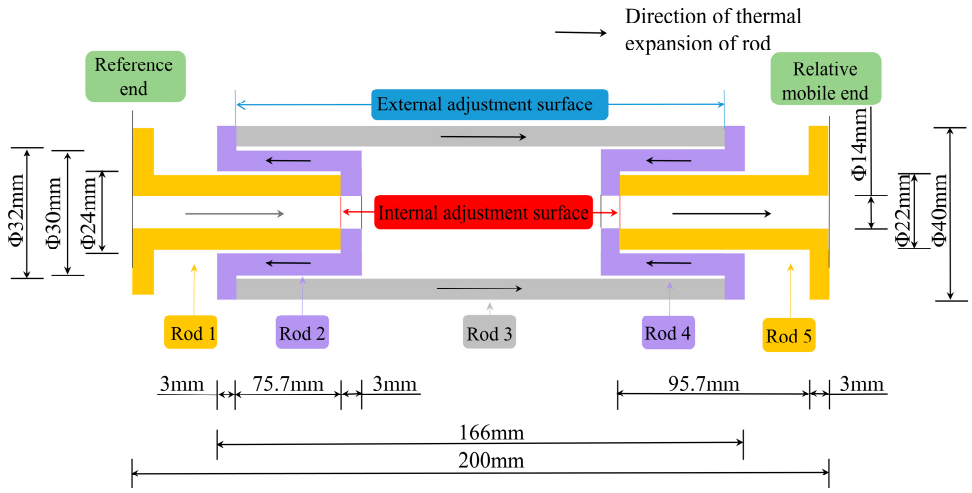

Figure 2. Schematic diagram of the thermal expansion support rod structure.

The design is a tube-like rod structure; due to the uniform temperature field, in order to facilitate the calculation, it will be made into a symmetrical design, that is, rod 1 and rod 5 and rod 2 and rod 4 are of the same length and material. Assuming that $\alpha_1, \alpha_2, \alpha_3, \alpha_4, \alpha_5$ is the CTE of rods 1, 2, 3, 4, and 5, one obtains $\alpha_1 = \alpha_5$, $\alpha_2 = \alpha_4$. Based on the geometric relationship, the following equation can be obtained:

$$\Delta l_T = \Delta l_1 - \Delta l_2 + \Delta l_3 - \Delta l_4 + \Delta l_5 \tag{2}$$

$$l_T = l_1 - l_2 + l_3 - l_4 + l_5 \tag{3}$$

$$l_1 = l_5 > l_2 = l_4 \tag{4}$$

$$\frac{1}{2} l_3 > l_2 \tag{5}$$

Δl_T is the displacement change for the linear thermal expansion of the overall rod; $\Delta l_1, \Delta l_2, \Delta l_3, \Delta l_4$ and Δl_5 is the displacement change for the linear thermal expansion of rod 1, rod 2, rod 3, rod 4, and rod 5, respectively; and l_1, l_2, l_3, l_4, l_5 is the length of rod 1, rod 2, rod 3, rod 4, and rod 5, respectively.

According to Equations (1)–(3), it can be seen that the larger the difference between the CTE of rod 2 α_2 and the sum of the CTE of rods 1 and 3 $\alpha_1 + \alpha_3$, the larger the difference in the lengths of the sub-rods and the larger the space of the design. At the same time, according to Equations (2), (4), and (5), it can be seen that if the support rod is to realize a negative coefficient of expansion, it has to satisfy $\alpha_2 > \alpha_1 + \alpha_3$. The CTE of the whole rod α_T can also be obtained as

$$\alpha_T = \frac{(l_1 + l_5)\alpha_1 - (l_2 + l_4)\alpha_2 + l_3\alpha_3}{l_T} \tag{6}$$

By choosing a material with a large difference in the CTE, i.e., satisfying $\alpha_2 > \alpha_1 + \alpha_3$ and, at the same time, taking into account the low or no magnetic moment and light weight, the aluminum alloy 7A09 and the titanium alloy TC4 are used as the support rod materials, i.e., $\alpha_{Ti} = \alpha_1 = \alpha_3 = \alpha_5$, $\alpha_{Al} = \alpha_2 = \alpha_4$. The connection structures at both ends of the support structure will undergo a displacement of 2×10^{-6} mm for a temperature change of 0.1 K. Additionally, given the distance between these two connection structures of 200 mm, it is required for the overall CTE of the entire rod to be -1×10^{-6}/K to compensate for this displacement when conducting the validation design for a support distance of 200 mm. A negative CTE means that when the temperature increases, the volume or length of the object shrinks. This means that many displacements caused by metal or other positive CTE materials due to temperature changes can be offset in the application of spatial support structures. According to the material properties of aluminum alloy 7A09 and titanium alloy TC4 provided by the materials' manufacturer, which are shown in Table 1, Equations (3)–(6) can be calculated to obtain the initial design values of each rod, which are $l_1 = l_5 = 95.7$ mm, $l_2 = l_4 = 75.7$ mm, and $l_3 = 160$ mm.

Table 1. The relevant material properties of aluminum alloy 7A09 and titanium alloy TC4.

Material	Elastic Modulus (GPa)	Density (g/cm^3)	Thermal Conductivity (W/(m·K))	CTE (1×10^{-6}/K)
7A09	7.1	2.8	142	23.6
TC4	10.9	4.44	7.4	9.6

By inserting them into Equation (6), it can be concluded that the CTE of the whole rod should be -0.998×10^{-6}/K.

2.2. Optimization of the Structure and Error Analysis

In the actual working condition of the support rod, the temperature change should satisfy (T ± 0.1)K/1000 s. However, in the actual simulation process, the displacement change under the temperature difference is too small, which makes the simulation result unreliable due to the computer calculation error. In order to avoid this problem, in the actual simulation process, the amount of the temperature change will be increased, so that the displacement caused by thermal deformation increases, and then the result will be divided by the corresponding temperature rise times to obtain the actual approximate results. Therefore, in the simulation, the temperature field is set to a uniform temperature field with a temperature rise of $\Delta K = 20$ K, i.e., the temperature change range is 20 °C~40 °C. According to the material properties of 7A09 and TC4 shown in Table 1, and the corresponding temperature change, the corresponding finite element model is established for calculation. Its grid model is shown in Figure 3. The minimum length of the elements in the model is 0.36486 mm, the maximum length is 1.13 mm, the minimum Jacobin is 0.72, and the maximum aspect ratio is 2.92. At the same time, the number of elements is 195,840. Due to the fact that the structure is inside a temperature-controlled box within the satellite, where the temperature changes very slowly and the thermal conduction within the structure is significant, we assume that the temperature is uniform across all nodes and the initial temperature is 20 °C. We directly apply the uniformly varying temperature field (20~40 °C) to all the nodes of the finite element model. Because the satellite experiences minimal gravitation in space, which can be almost entirely neglected, the structure is essentially free from any external payloads. Additionally, the pressure inside the temperature-controlled box has little to no impact on the structure. Therefore, we do not apply any forces or pressure within the model. And the thermal conduction at the contact surfaces of the structural components is also direct conduction. And one end of the rod is limited to only one degree of freedom of the axial displacement. The simulation solution is carried out by using the OptiStruct of HyperMesh in hyperworks.

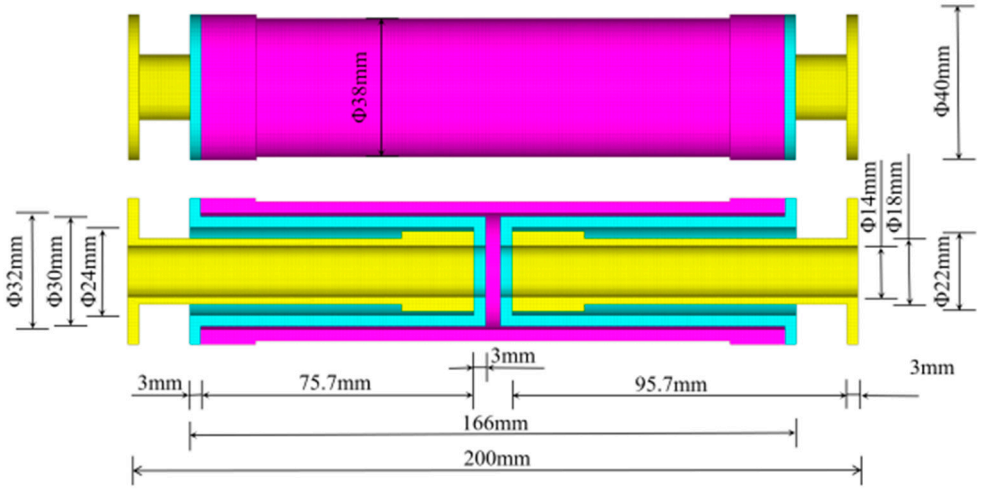

Figure 3. Proportional grid model of the support rod.

However, due to the different CTEs of titanium alloy and aluminum alloy, a certain amount of stress will be generated, which will lead to a certain amount of strain in the rod, which will in turn affect the displacement accuracy of the whole rod. As shown in Figure 4, if the initial value of the above equation is directly adopted, the relative displacement of the two ends is -5.351798×10^{-6} mm. According to Equation (1), the CTE of the whole rod can be obtained as $-1.3379495 \times 10^{-6}$/K, which is 34.06% different from the theoretical data.

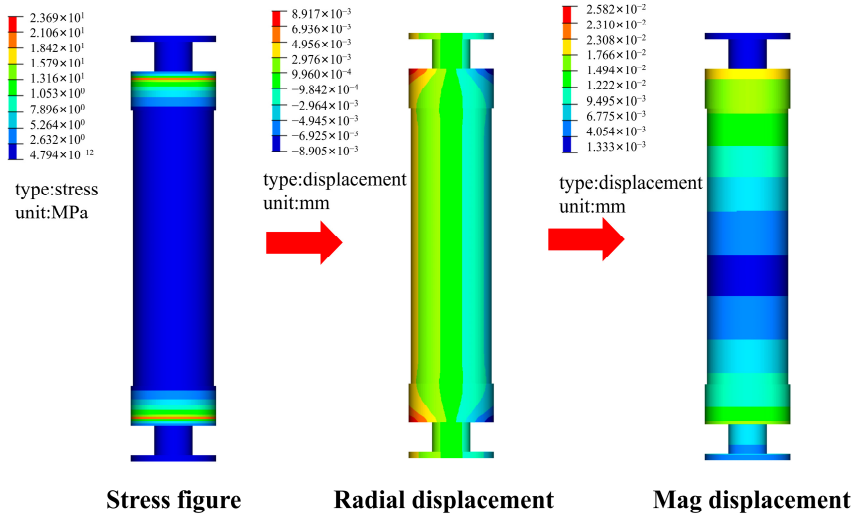

Figure 4. Schematic diagram of strain due to radial stresses.

In order to achieve the desired accuracy, we optimize the structure by using the optimization method of the NLPQL with the objective of the CTE as -1×10^{-6}/K, i.e., the relative displacement of the two ends reaches -4×10^{-3}mm for optimization. The optimization process is shown in Figure 5.

Assuming that the distance between the internal and external adjustment surfaces is the design variable $x = (x_1, x_2)$, the final optimized result is $\begin{cases} x_1 = 10.35579071 \text{ mm} \\ x_2 = 160.001 \text{ mm} \end{cases}$.

Due to the precision of processing, after rounding off the length of each rod, the final results are $l_1 = l_5 = 94.8$ mm, $l_2 = l_4 = 74.8$ mm, and $l_3 = 160$ mm. Its final thermal deformation is -0.004032286 mm, and the CTE is $-1.0080715 \times 10^{-6}$/K.

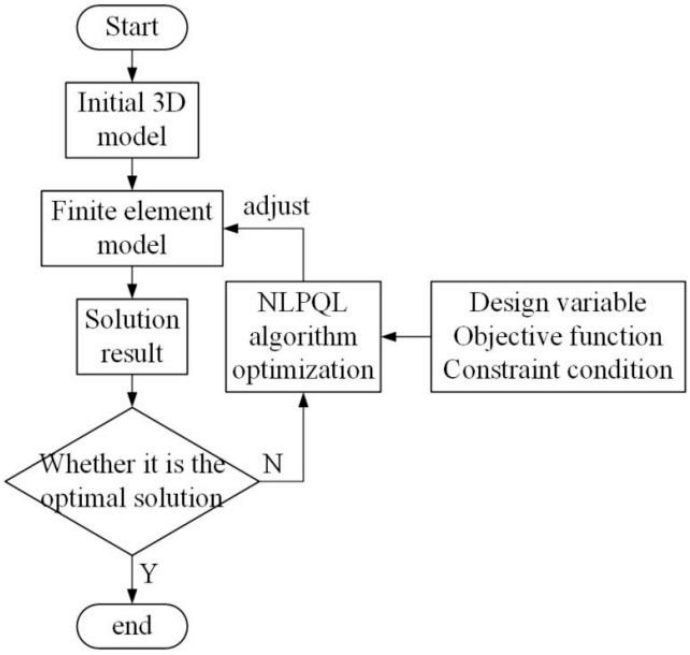

Figure 5. Flowchart of the optimization process of the whole rod structure.

Because there may be some errors in the measurement data of the CTE of the material due to the measuring instruments in the actual measurement process, the DOE full factorial design method [21] is utilized to sample the possible errors. We take the CTE of two materials within the range of ±5%, with 1% as a sampling interval. The results of the response surface are shown in Figure 6. In the temperature difference in a 20-degree range, the displacement of the two ends of the whole rod and the relative change in the CTE of the two materials have a certain proportionality, that is, the CTEs of the two materials at the same time increase or decrease; a certain percentage of the thermal deformation of the whole rod displacement change is relatively small, while the two materials produce a relative change in the thermal deformation of the whole rod which will produce a huge change in the displacement of the thermal deformation of the whole rod. The figure confirms Equation (6), that is, the influence of the thermal expansion coefficient of each rod on the whole rod.

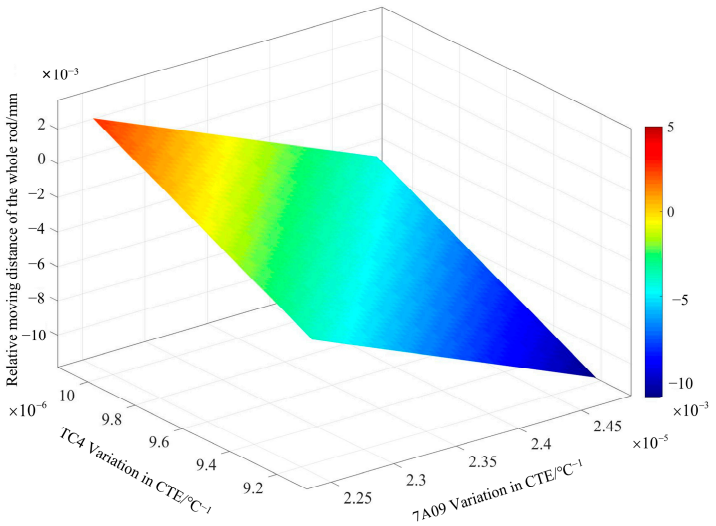

Figure 6. Error response plot from variation in the CTE.

3. The Thermal Stability Experiment and Results Analysis for the Support Structure

This experiment mainly involves two aspects: one is temperature control, and the other is displacement measurement. For these two aspects, we establish both the environmental temperature control system and the displacement interference monitoring system. Moreover, the uniformity of the environmental temperature is verified. Meanwhile, the relationship curves between temperature and displacement are measured under the same time scale, and some analyses are carried out on this result.

3.1. Environmental Temperature Control System

For the experiments of building the environment, we use a polyethylene foam material for insulation with a thermal conductivity of 0.06 W/(m·K). Because we use sealing tape to seal it, there is almost no outward gas exchange during the experiment. The internal gas temperature rise is only related to the power of the heating films in the experimental box and the heat exchange between the box shell and the outside world.

In this experiment, the size of the test box is 450 mm × 450 mm × 195 mm, its heat dissipation area is 756,000 mm^2, and the thickness of its box is 20 mm. The heat dissipation from the thermal insulation test box can be considered as the conduction heat exchange within the shell of the box, according to the conduction heat exchange in Equation (7):

$$Q = \frac{\lambda S}{\delta} \Delta T \tag{7}$$

Q is the rate of heat transfer, λ is the thermal conductivity of the material, S is the contact area, δ is the thickness of the material, and ΔT is the temperature difference between the two ends. If the relevant parameters are inserted into the equation, the heat transfer from its case to the outside world is obtained as 45.36 W. Because the specifications of the heating films on both sides should be the same, in order to reduce the possible uneven temperature field, selecting two 25 W polyimide heating films, totaling 50 W of heating power, therefore aligns closely with the calculated specifications. The heat generated by the polyimide heating films can quickly spread to the surrounding air, but if we do not speed up the heat exchange of the surrounding gas, the box will produce a relatively large temperature difference inside; thus, in order to speed up the gas exchange, a fan is added to the area surrounding each of the heating films in the chamber of the experimental box. The fans should aim at each heating film to blow on them. At the same time, in order to prevent heat concentration on the test piece due to the fan blowing out directly, two windbreaks are utilized to isolate the heating film from the fan as well as to make the fan blow air toward the heating film. The position relationship of the devices in the experimental box is shown in Figure 7.

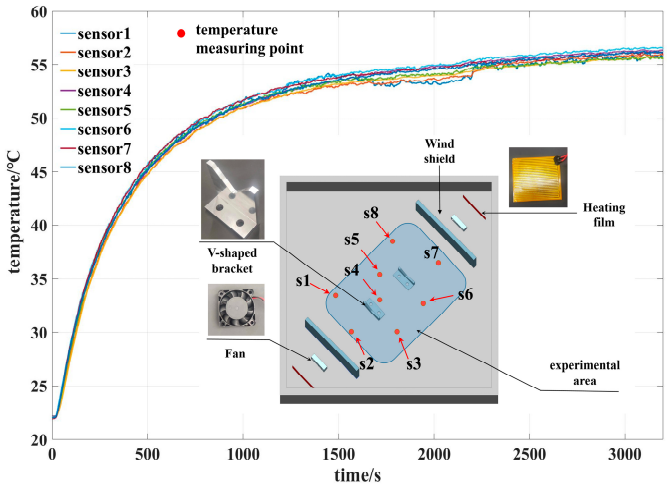

Figure 7. A schematic representation of the arrangement of components inside the experimental box and a temperature test results graph.

Eight PT100 RTD temperature sensors are randomly and uniformly distributed in the test area. The test data show that the temperature stabilization of its temperature difference is about ±0.5 K in the experimental region during the temperature rise process. In order to test the effect of temperature uniformity in the box on the rod under test, the aluminum alloy rod and titanium alloy rod are put into the test box before the formal experiment starts, and the temperature sensors are uniformly attached inside and outside the rod to monitor the temperature change. Due to the small size of the aluminum alloy rod, only six detectors are used, while the titanium alloy rod is monitored by eight detectors. The positional relationship between the temperature sensors and the rod under test during the experiment is shown in Figures 8 and 9.

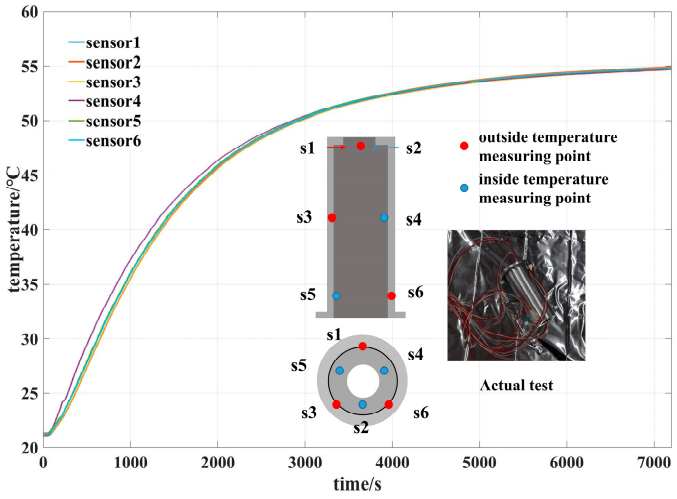

Figure 8. Temperature measurement position and temperature test results of aluminum alloys.

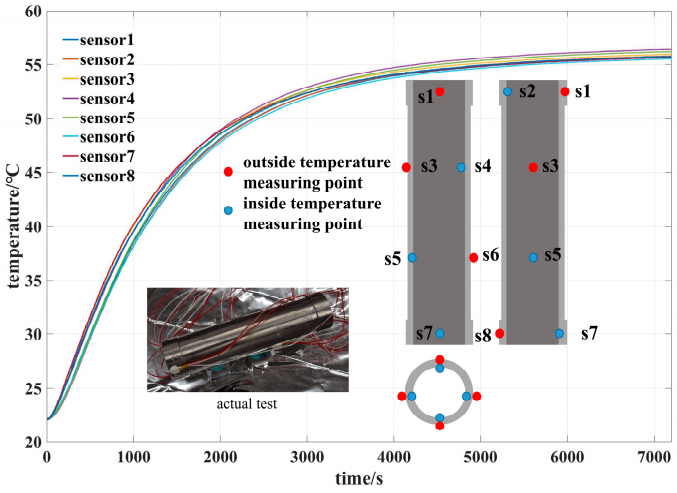

Figure 9. Temperature measurement position and temperature test results of titanium alloys.

According to Figures 8 and 9, when the temperature in the experimental box has reached equilibrium, the temperature difference in the aluminum alloy in the equilibrium state is less than ±0.3 K, and when the temperature difference in the titanium alloy is less than ±0.5 K, it shows that the uniform distribution of the temperature field is basically achieved in the rod.

3.2. The Displacement Interferometric Monitoring System

In the displacement measurement system, we use a fiber-based interferometer to measure the displacement of both ends of the rod due to thermal deformation, which is

more convenient and more accurate than using a Michelson interferometer in a complex atmospheric environment [22].

The measurement process of the fiber-based interferometer is shown in Figure 10.

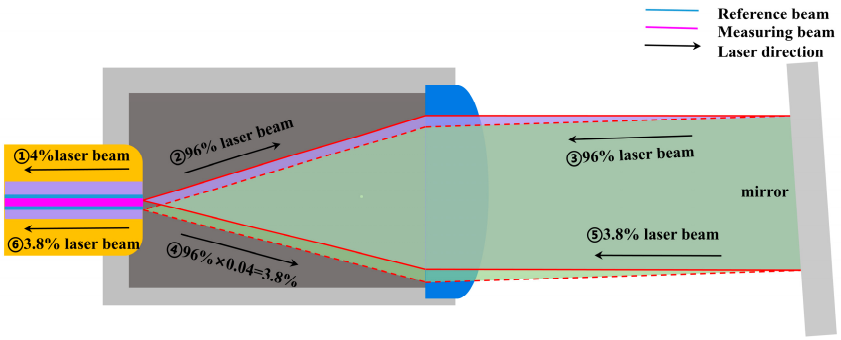

Figure 10. Principle schematic diagram of the fiber-based interferometer.

At first, the initial laser is directly reflected back by the fiber end face with 4% of the laser to the fiber core as a reference beam (E_r, while the remaining 96% of the laser passes through the connector surface and is reflected by the mirrors to focus on the connector surface. Approximately 4% of this beam (i.e., 96% × 4% = 3.84% of the laser) is again reflected by the connector surface and will finally be reflected by the mirrors to focus on the fiber core to form the measurement beam (E_m). The beams E_r and E_m are described by the following equations, Equations (8) and (9) [12,22].

$$E_r = A_r e^{-i\Phi_r} e^{i2\pi f_r t} \tag{8}$$

$$E_m = A_m e^{-i\Phi_m} e^{i2\pi f_m t} \tag{9}$$

A_r and A_m are the amplitude factors, Φ_r and Φ_m are the phase factors, and f_r and f_m are the frequency factors. The response of the detector to the interfering beam is described in (10), and O_{Dect} is the quantity of the optical intensity detected by the detector [12]. Because the process is zero-difference interferometry, both beams have the same frequency, so $f_r = f_m$. Assuming that the phase difference between the two beams is $\Delta\Phi = \Phi_r - \Phi_m$, the displacement Δx can be obtained according to Equation (11) as long as the phase difference $\Delta\Phi$ is detected.

$$O_{Dect} = 2A_r A_m \cos(2\pi(f_r - f_m)\cdot t - (\Phi_r - \Phi_m)) \tag{10}$$

$$\Delta x = \frac{4\pi}{\lambda}\Delta\Phi \tag{11}$$

In the process of displacement measurement, with the change in temperature inside the insulation box, the environment inside the box, such as the humidity and pressure, will change. And the temperature, humidity, and pressure will cause a change in the air refractive index [23]. In order to minimize the influence of the change in the air refractive index on the displacement measurement, the environmental compensation unit (ECU) is introduced to compensate for the change in environmental factors, and the ECU calculates the air refractive index by collecting the information on the surrounding environment using the indirect measurement method [24,25].

In order to ensure that an interference path can be formed between the two end faces of the measuring rod, we design a simple flexible structure for fixing and adjusting the position of the reflector, which is made of invar, a material with a low CTE, which is 0.7×10^{-7}/K. The reflective surface of the mirror is also aligned with the measuring end of the rod as much as possible to minimize the effect of the structure on the measurement results. Meanwhile, in order to ensure the effectiveness of the flexible structure, a forced

displacement of 0.01 mm is applied to it under the simulation condition, and its maximum stress is 24 Mpa, which is much smaller than the yield limit of invar, 276 Mpa. The structural diagram of the assembly of the flexible structure and the rod and the simulation results are shown in Figure 11.

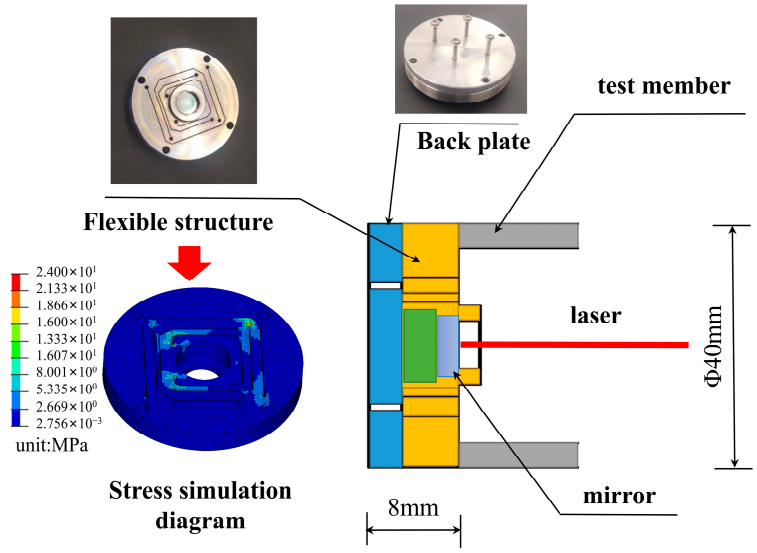

Figure 11. Schematic diagram of the assembly position of the flexible structure.

3.3. The Experimental Process and Analysis Results

During the formal experiment, after removing some temperature sensors in each rod to be tested, the fiber-based interferometer is installed on one side of the rod to be tested, and the reflector is installed on the other side. The positional relationship diagram is shown in Figure 12.

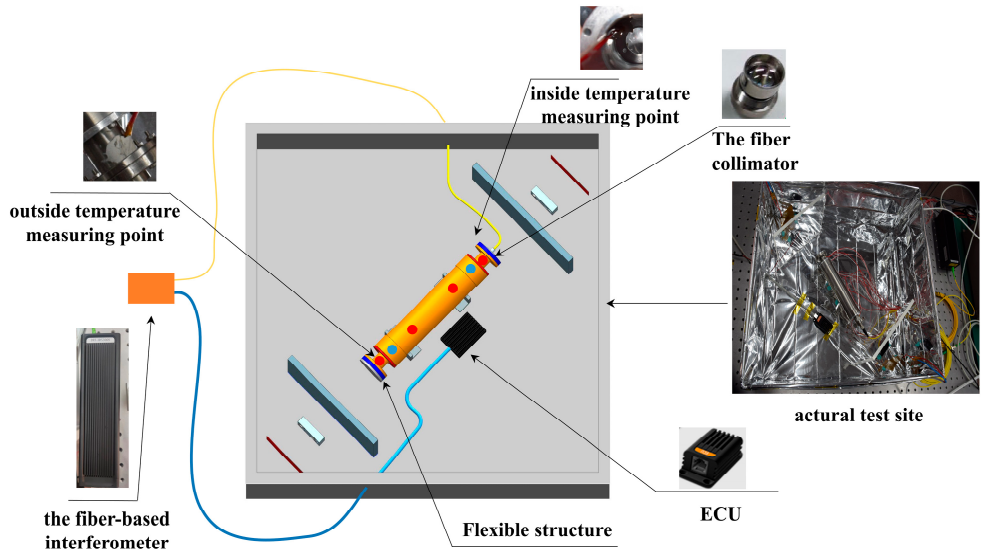

Figure 12. Overall experimental schematic.

After installing the equipment, due to the large gap between the temperature sensor and the fiber-based interferometer sampling time interval, it is necessary to perform some unification of their sampling time interval. The sampling interval of the interferometer is 0.001 s, while that of the temperature sensor is 0.1 s, so we use a sampling interval of 0.1 s. At the same time, in order to ensure the accuracy of the measurement of the CTE of the experimental materials and to verify the accuracy of the measurement system,

we first perform some measurements on the titanium alloy rods and aluminum alloy rods in order to verify the thermal expansion properties of the materials provided by the materials' manufacturers. The thermal expansion–displacement curves of titanium alloy and aluminum alloy are shown in Figures 13 and 14.

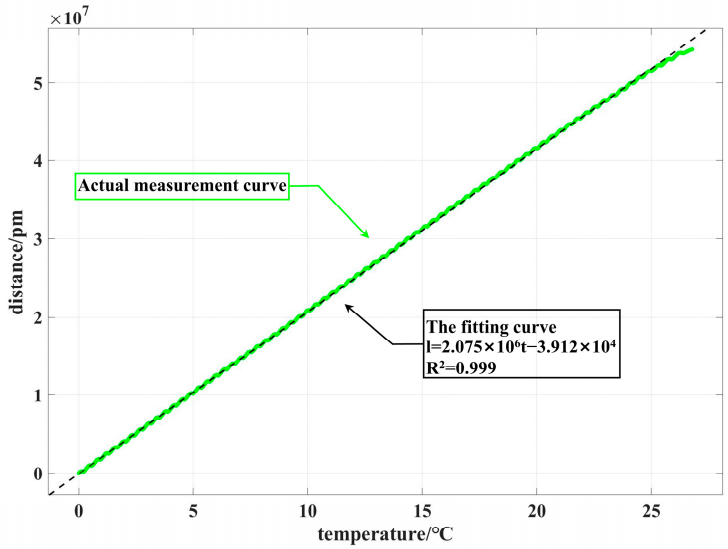

Figure 13. The thermal expansion–displacement curve of aluminum alloy.

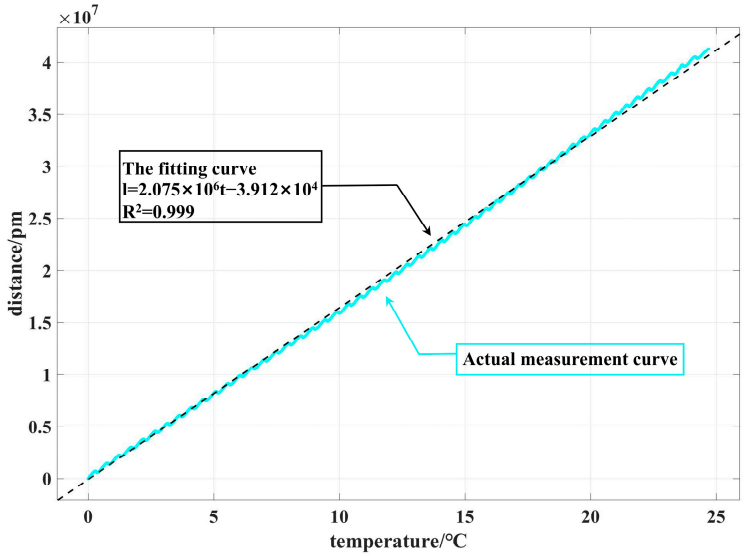

Figure 14. The thermal expansion–displacement curve of titanium alloy.

The CTE of the material is known to be constant over a range of temperatures. Therefore, we assume that the linear regression equation for the curve is $\hat{l} = \hat{a} + \hat{b}t$. According to the linear regression equation, we solve Equations (12) and (13):

$$\hat{b} = \frac{\sum_{i=1}^{n} t_i l_i - n\bar{t}\bar{l}}{\sum_{i=1}^{n} t_i^2 - n\overline{t^2}} \tag{12}$$

$$\hat{a} = \bar{l} - \bar{t}\hat{b} \tag{13}$$

In the above two equations, $\hat{a}$ and $\hat{b}$ are the parameters to be determined and n is the number of sampled data points. Therefore, by substituting the measurement data into the

equations, we can obtain the linear regression equations for the temperature–displacement curves of titanium alloy and aluminum alloy as follows:

$$l = 1.649 \times 10^6 t - 7.387 \times 10^4 \tag{14}$$

$$l = 2.075 \times 10^6 t - 3.912 \times 10^4 \tag{15}$$

According to the equation for calculating the coefficient of determination,

$$R^2 = \frac{\sum_{n=1}^{n} \left(\hat{l} - \bar{l}\right)^2}{\sum_{i=1}^{n} \left(l_i - \bar{l}\right)^2} \tag{16}$$

The coefficients of determination of titanium alloy and aluminum alloy can be obtained as $R^2 = 0.9993$ and $R^2 = 0.9999$, respectively. It is known that the actual length of the measured titanium alloy rod is 170 mm, and the actual length of the aluminum alloy rod is 88 mm. Bringing Equations (14) and (15) into Equation (1), the CTE of titanium alloy can be obtained as 9.7×10^{-6}/K and the CTE of aluminum alloy can be obtained as 23.57×10^{-6}/K, which is basically the same as that of the data provided by the manufacturer. Therefore, the size of each rod is first adjusted to a predetermined value, after which it is assembled and measured. The experimental results are shown in Figure 15:

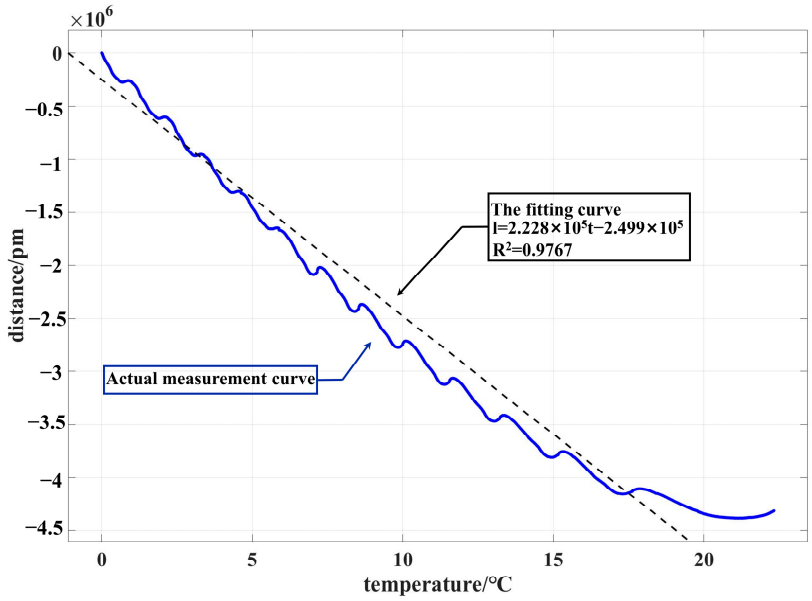

Figure 15. The thermal expansion–displacement curve of the whole rod.

Bringing the data into Equations (12) and (13) gives the linear regression equation for the whole rod as

$$l = -2.228 \times 10^5 t - 2.499 \times 10^5 \tag{17}$$

And its coefficient of certainty is $R^2 = 0.9767$. The experimental results, as shown in Figure 14, show that the temperature–displacement change curve of the whole rod has a concave trend in the process of the temperature rise, resulting in the slope of the fitted curve being larger than the measured results, which may be caused by the aluminum alloy thermal conductivity efficiency being faster than that of titanium alloy, so the actual value should be closer to the theoretical and simulation values. Bringing Equation (17) into Equation (1), the CTE of the whole rod is -1.114×10^{-6}/K, which is 9.5% different from the simulation results ($-1.0080715 \times 10^{-6}$/K) and basically meets the design requirements.

4. Conclusions

In the Chinese Taiji Program, the support structure between the payloads requires high thermal stability and low or no magnetic moments. In order to meet these requirements, a support rod with a CTE of -0.998×10^{-6}/K was designed by using titanium alloy and aluminum alloy, and the optimized CTE was $-1.0080715 \times 10^{-6}$/K. The CTE of -1.114×10^{-6}/K was verified by the experiments, which is 9.5% different from the simulation results, and the feasibility of this design was verified. This result essentially meets the Taiji Program's requirement for a whole 200 mm support rod with a CTE of -1×10^{-6}/K.

Next, we will delve deeper into the stress and strain mechanisms resulting from the different CTEs of each material, aiming to further enhance the thermal stability of the support structure. Following this, the final support structure will be integrated into a satellite for comprehensive testing, validating its thermal and dimensional stability within a real-world environment.

In conclusion, this study provides a useful exploration and theoretical basis for the design and optimization of the support rods in the gravitational wave detection project of the Taiji Program, which provides strong support for the successful implementation of the project. In the future, we will further improve the material properties and optimize the structural design to achieve higher precision and stability for the support rod so as to contribute to the field of gravitational wave detection.

Author Contributions: Conceptualization, Y.D.; methodology, Y.D.; software, Y.D.; validation, W.S. and W.T; formal analysis, Y.D.; investigation, Y.D.; resources, Y.D.; data curation, Y.D.; writing—original draft preparation, Y.D.; writing—review and editing, W.S.; visualization, Y.D.; supervision, W.S.; project administration, W.T.; funding acquisition, X.D. All authors have read and agreed to the published version of the manuscript.

Funding: This work was supported by the National Key Research and Development Program of China under grant 2020YFC2201300.

Data Availability Statement: The data presented in this study are available from the corresponding author upon request. The data are not publicly available due to privacy restrictions.

Conflicts of Interest: The authors declare no conflict of interest.

References

1. Liu, Y. The Detection Scheme and Applications of Gravitational Waves. *Highlights Sci. Eng. Technol.* **2023**, *48*, 212–217. [CrossRef]
2. Ziren, L.; Yan, W.; Yueliang, W.; Wenrui, H.; Gang, J. The Taiji program: A concise overview. *Prog. Theor. Exp. Phys.* **2020**, *2021*, 05A108.
3. Baghi, Q.; Karnesis, N.; Bayle, J.B.; Besançon, M.; Inchauspé, H. Uncovering gravitational-wave backgrounds from noises of unknown shape with LISA. *J. Cosmol. Astropart. Phys.* **2023**, *4*, 066. [CrossRef]
4. Abbott, B.P. Observation of gravitational waves from a binary black hole merger. *Phys. Rev. Lett.* **2017**, *116*, 061102. [CrossRef]
5. Szekerczes, K.; Noble, S.; Chirenti, C.; Thorpe, J.I. Imaging the Milky Way with Millihertz Gravitational Waves. *Astron. J.* **2023**, *166*, 17. [CrossRef]
6. Abramovici, A.; Althouse, E.W. LIGO: The Laser Interferometer Gravitational-Wave Observatory. *Science* **1992**, *256*, 325–333. [CrossRef] [PubMed]
7. Sha, W.; Fang, C.; Niu, Y. Successful application of optical bench in Taiji-1 laser interferometer. *Int. J. Mod. Phys. A* **2021**, *36*, 2140001. [CrossRef]
8. Merkowitz, S.M.; Conkey, S.; Haile, W.B.; Kelly, W.R., III; Peabody, H.; Dumont, P.J. Structural, thermal, optical and gravitational modelling for LISA. *Class. Quantum Gravity* **2004**, *21*, S603. [CrossRef]
9. Saulson, P.R. *Fundamentals of Interferometric Gravitational Wave Detectors*; World Scientific: Singapore, 1994.
10. Gao, H. Method to Remove Tilt-to-Length Coupling Caused by Interference of Flat-Top Beam and Gaussian Beam. *Appl. Sci.* **2019**, *9*, 4112.
11. Luo, Z.; Guo, Z.K.; Jin, G.; Wu, Y.; Hu, W. A brief analysis to Taiji: Science and technology. *Results Phys.* **2019**, *16*, 102918. [CrossRef]
12. Sang, B.; Deng, X.; Peng, B.; Tao, W.; Sha, W. Dimensional Stability Ground Test and in-Orbit Prediction of SiC Telescope Frame for Space Gravitational Wave Detection. *IEEE Access* **2022**, *10*, 21041–21047. [CrossRef]

13. Luo, Z.; Liu, H.; Jin, G. The recent development of interferometer prototype for Chinese gravitational wave detection pathfinder mission. *Opt. Laser Technol.* **2018**, *105*, 146–151. [CrossRef]
14. Mohammed, A.; Boudjemai, A.; Chouraqui, S.; Benyettou, M. Magnetorquer Control for Orbital Manoeuvre of Low Earth Orbit Microsatellite. *World Sci. Eng. Acad. Soc. (WSEAS)* **2006**, *5*, 944–947.
15. Ludlam, M.; Angelopoulos, A.; Taylor, E.; Snare, R.C.; Means, J.D.; Ge, Y.S.; Narvaez, P.; Auster, H.U.; Le Contel, O.; Larson, D.; et al. The THEMIS Magnetic Cleanliness Program. *Space Sci. Rev.* **2008**, *141*, 171–184. [CrossRef]
16. Song, W.; Xie, P.; Liu, S.; Xie, Y. Thermal Stability Design of Asymmetric Support Structure for an Off-Axis Space Camera. *Appl. Sci.* **2021**, *11*, 11. [CrossRef]
17. Sandin, C.R.; Allen, L.N.; Amatucci, E.G.; Arenberg, J.W.; Carter, R.C.; Corsetti, J.A.; DiPirro, M.J.; East, M.; Fantano, L.G.; Flores, A.; et al. Materials evaluation for the origins space telescop. *J. Astron. Telesc. Instrum. Syst.* **2021**, *7*, 1. [CrossRef]
18. Lu, B.; Wang, F.; Zhang, B. Design of a Dynamic Secondary Mirror Truss Adjustment Mechanism for Large Aperture Telescopes. *Appl. Sci.* **2023**, *13*, 1058. [CrossRef]
19. Liu, H.; Zhang, X.F.; Feng, J.C.; Zhu, C.; Cai, Z.M.; Xu, Y. Application of precision thermal controll techniques in Taiji-1 satellite. *Chin. J. Space Sci.* **2021**, *41*, 5. (In Chinese) [CrossRef]
20. Schittkowski, K. NLPQL: A FORTRAN subroutine solving constrained nonlinear programming problems. *Ann. Oper. Res.* **1986**, *5*, 485–500. [CrossRef]
21. Uebelhart, S.; Miller, D. Uncertainty evaluation for parameterized spacecraft architectures in conceptual design. In Proceedings of the 48th AIAA/ASME/ASCE/AHS/ASC Structures, Structural Dynamics, and Materials Conference, Honolulu, HI, USA, 23–26 April 2007; p. 2373.
22. Thurner, K.; Quacquarelli, F.P.; Braun, P.F.; Dal Savio, C.; Karrai, K. Fiber-based distance sensing interferometry. *Appl. Opt.* **2015**, *54*, 3051–3063. [CrossRef]
23. Owens, J.C. Optical refractive index of air: Dependence on pressure, temperature and composition. *Appl. Opt.* **1967**, *6*, 51–59. [CrossRef] [PubMed]
24. Lazar, J.; Číp, O.; Čížek, M.; Hrabina, J.; Buchta, Z. Interferometry with direct compensation of fluctuations of refractive index of air. In Proceedings of the 17th Slovak-Czech-Polish Optical Conference on Wave and Quantum Aspects of Contemporary Optics, Liptovsky Jan, Slovakia, 6–10 September 2010; Volume 7746, pp. 125–130.
25. Dvořáček, F. Survey of selected procedures for the indirect determination of the group refractive index of air. *Acta Polytech.* **2018**, *58*, 9–16. [CrossRef]